

NANO EXPRESS

Open Access



# Enhanced Biocompatibility in Anodic TaO<sub>x</sub> Nanotube Arrays

Yu-Jin Zeng<sup>1</sup>, Sheng-Chen Twan<sup>1</sup>, Kuan-Wen Wang<sup>1</sup>, Her-Hsiung Huang<sup>2</sup>, Yen-Bin Hsu<sup>3,4</sup>, Chien-Ying Wang<sup>5</sup>, Ming-Ying Lan<sup>3,4\*</sup> and Sheng-Wei Lee<sup>1\*</sup>

## Abstract

This study first investigates the biocompatibility of self-organized TaO<sub>x</sub> nanotube arrays with different nanotube diameters fabricated by electrochemical anodization. All as-anodized TaO<sub>x</sub> nanotubes were identified to be an amorphous phase. The transition in surface wettability with TaO<sub>x</sub> nanotube diameters can be explained based on Wenzel's model in terms of geometric roughness. In vitro biocompatibility evaluation further indicates that fibroblast cells exhibit an obvious wettability-dependent behavior on the TaO<sub>x</sub> nanotubes. The 35-nm-diameter TaO<sub>x</sub> nanotube arrays reveal the highest biocompatibility among all samples. This enhancement could be attributed to highly dense focal points provided by TaO<sub>x</sub> nanotubes due to higher surface hydrophilicity. This work demonstrates that the biocompatibility in Ta can be improved by forming TaO<sub>x</sub> nanotube arrays on the surface with appropriate nanotube diameter and geometric roughness.

**Keywords:** Biocompatibility, TaO<sub>x</sub> nanotubes, Anodic oxidation, Hydrophilicity, Human fibroblast cells

## Background

Tantalum (Ta) is a rare, hard, highly corrosion-resistant, and bioinert metal [1–3]. Oxidation of the tantalum material, by forming a very thin, impenetrable oxide film on its surface, contributes to its biocompatibility. The high flexibility and biocompatibility of tantalum render its clinical applications, such as dental implants, orthopedic implants, and bone reconstruction [4–6]. Recently, tantalum was found to have better biocompatibility than titanium, such as more abundant extracellular matrix formation, excellent cellular adherence and growth, and a much higher living cell density on the surface [7–9]. On the other hand, several studies have proved that the distinctive physico-chemical property of nanostructured surface geometry is the main factor influencing cell behavior [10–12]. The ideal biomaterial surface should be able to provide the optimal environment for cell in-growth. Ruckh et al. demonstrated that anodized Ta nanotubes provide a substrate for enhanced osseointegration when compared to flat surface [13]. A recently

developed porous tantalum material, mimicking the properties of bone, allows the soft tissue and bone in-growth which provides good biological fixation [14–17]. The high stability and healing potential of porous tantalum help to fuse the gaps between bone structures during reconstructive surgery. The porous tantalum thus regained much interest in the biomaterial field due to its several advantages compared to other grafts, such as no donorsite morbidity, high stability, excellent osseointegrative properties, and prevention of potential risk of transmission of infectious diseases [18–21]. A recent clinical review showed that patients who received porous tantalum acetabular cups had a higher degree of implant fixation compared to those with hydroxyapatite-coated titanium (Ti) cups [22–25].

Recently, we have developed self-organized TiO<sub>2</sub> nanotubes with different diameters by utilizing an electrochemical anodization method [26, 27]. We found that human fibroblast cells show more obvious diameter-specific behavior on the supercritical CO<sub>2</sub> (ScCO<sub>2</sub>)-treated nanotubes than those on the as-anodized ones [27]. We further fabricated Ag-decorated TiO<sub>2</sub> nanotubes by the electron-beam evaporation method and found the smallest diameter (25-nm-diameter) Ag-decorated nanotubes exhibited the most

\* Correspondence: mingyinglan@gmail.com; swlee@g.ncu.edu.tw

<sup>3</sup>Department of Otolaryngology Head and Neck Surgery, Taipei Veterans General Hospital, Taipei 112, Taiwan, Republic of China

<sup>1</sup>Institute of Materials Science and Engineering, National Central University, Taoyuan 320, Taiwan, Republic of China

Full list of author information is available at the end of the article

obvious biological activity in promoting adhesion and proliferation of human fibroblasts and also human nasal epithelial cells [26]. In this study, we fabricated TaO<sub>x</sub> nanotubes with different diameters by the similar electrochemical anodization method. The cell behavior, including cell adhesion, and proliferation, in response to the diameter of TaO<sub>x</sub> nanotubes were investigated. The objective of this research is to study the biocompatibility of self-organized TaO<sub>x</sub> nanotube arrays with different nanotube diameters fabricated by electrochemical anodization.

## Methods

### Preparation of TaO<sub>x</sub> Nanotubes

Ta sheets were purchased from ECHO Chemical (thickness of 0.127 mm, 99.7% purity, CAS No. 7440-25-7). Before the anodization process, Ta sheets were ultrasonically cleaned in acetone, isopropanol, ethanol, and water. All anodization experiments were performed at 20 °C in sulfuric acid solution containing 4.9 wt% HF, which was prepared from reagent-grade chemicals and deionized water. A two-electrode electrochemical cell with Ta as the anode and Pt as the counter electrode was employed. The voltages were adjusted from 10 to 40 V to result in TaO<sub>x</sub> nanotube diameters ranging from 20 up to 90 nm. Low-intensity UV-light irradiation (about 2 mW/cm<sup>2</sup>) with fluorescent black-light bulbs on TaO<sub>x</sub> nanotube samples for 8 h was done before the biocompatible tests.

### Material Characterization

The surface morphology, inner and outer diameter, wall thickness, and length of TaO<sub>x</sub> nanotubes were characterized by scanning electron microscopy (SEM). X-ray diffraction (XRD) and transmission electron microscopy (TEM) equipped with an energy dispersion spectrometer (EDS) were employed to examine the crystalline structure of the TaO<sub>x</sub> nanotube arrays. Contact angle measurements were carried out to evaluate the surface wettability of the TaO<sub>x</sub> nanotube samples by the extension method using a horizontal microscope with protractor eyepiece. Water and culture medium were used as test liquids for the measurements.

### Human Fibroblast Cell Culture

MRC-5 human fibroblasts (BRCC, Bioresource Collection and Research Center, Hsinchu, Taiwan, BCRC No. 60023) were plated in 10-cm tissue culture plate and cultured with Eagle's minimum essential medium (Gibco) containing 10% fetal bovine serum (FBS), 2 mM L-glutamine, 1.5 g/L sodium bicarbonate, 0.1 mM non-essential amino acids, and 1.0 mM sodium pyruvate and in 5% CO<sub>2</sub> at 37 °C. Cells were then seeded on to the autoclaved TaO<sub>x</sub> sheets placed on the bottom of 12-well culture plate (Falcon) for further study.

### Cell Adhesion Assay

Cells were seeded on each TaO<sub>x</sub> sheet at a density of  $2.5 \times 10^3$  cells/cm<sup>2</sup> and incubated in 5% CO<sub>2</sub> at 37 °C for 3 days and rinsed twice with PBS. The adherent cells on the substrate were fixed for 1 h in 4% paraformaldehyde at room temperature, followed by two washes in phosphate buffered saline (PBS) and permeabilization with 0.1% Triton X-100 (Sigma-Aldrich) in PBS for 15 min at 4 °C. After washing with PBS, the actin filament was labeled by incubating with rhodamine phalloidin (Life Technologies) at room temperature for 15 min. Then cell nuclei were stained by incubating with diamidino-2-phenylindole (DAPI) (Thermo Fisher Scientific) for 5 min. Cells were analyzed under a fluorescent microscope (AX80, Olympus) to examine the cell adhesion morphology and cytoskeletal arrangement. For SEM observation, cells were fixed with 2.5% glutaraldehyde solution (Merck) for 1 h at room temperature, then rinsed in PBS solution twice, dehydrated in a series of ethanol (40, 50, 60, 70, 80, 90, and 100%) and critical point dried with a critical-point dryer (CPD 030, Leica). A thin platinum film was coated on the samples before SEM observation.

### Cell Proliferation Assay

Cells were seeded on each TaO<sub>x</sub> substrates at density of  $1 \times 10^4$  cells/cm<sup>2</sup> and cultured for 1 week. After 1 week, the samples were rinsed with PBS twice and the cell proliferation was estimated by using WST-1 reagent kit (Roche, Penzberg, Germany). The medium containing 10% WST-1 cell proliferation reagent was added to each specimen and incubated in humidified atmosphere of 5% CO<sub>2</sub> at 37 °C for 2 h. The solution of each well were transferred to a 96-well plate. The absorbance of solution was measured at 450 nm using the spectrophotometer (Spectral Max250).

### Statistical Analysis

All experiments were carried out in triplicate, and at least three independent experiments were performed. Data were presented as mean  $\pm$  standard deviation (SD) and analyzed by analysis of variances (ANOVA) using SPSS 12.0 software (SPSS Inc.). A *p* value of < 0.05 was considered statistically significant.

## Results and Discussion

Figure 1a–e shows the SEM images of the flat Ta foil and as-anodized TaO<sub>x</sub> nanotube arrays with an average nanotube diameter of 20, 35, 65, and 90 nm, respectively. All as-anodized TaO<sub>x</sub> nanotubes exhibit well-defined nanotubular structure, and their nanotube diameters were nearly proportional to the applied voltages. Among these samples, the 20-nm-diameter nanotubes show relatively unclear nanotubular surface,

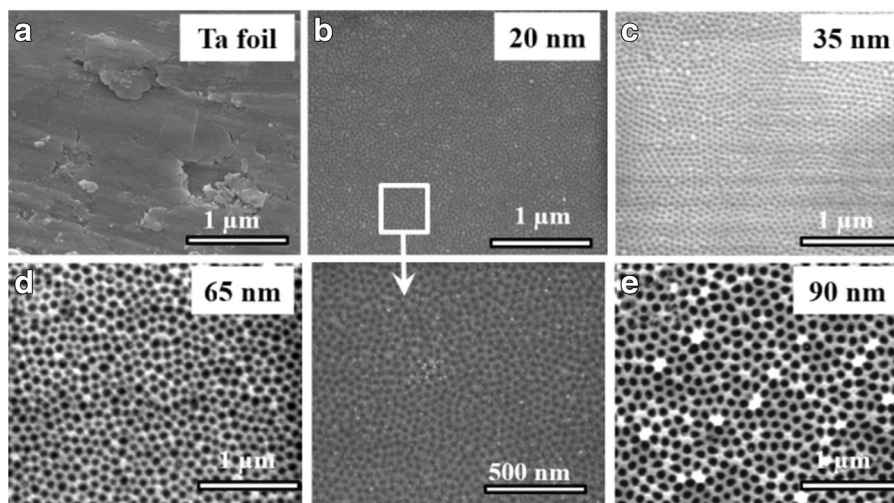


**Fig. 1** SEM images showing the **a** Ta foil surface and self-organized TaO<sub>x</sub> nanotubes with diameters of **b** 20, **c** 35, **d** 65, and **e** 90 nm, respectively

as shown in the enlarged area taken from Fig. 1b. This observation can be attributed to the weaker field strength under low-voltage operation in the anodization process. Figure 2 further shows the cross-section of all TaO<sub>x</sub> nanotubes and their corresponding nanotubular lengths. XRD and TEM analyses were employed to further identify the TaO<sub>x</sub> nanotube crystallinity. As

shown in the XRD spectra of Fig. 3a, only peaks related to the Ta foil are observed (JCPDS Card no. 04–0788), suggesting that as-anodized TaO<sub>x</sub> nanotubes are possibly amorphous phase. Figure 3b shows a representative TEM image taken from a 90-nm-diameter TaO<sub>x</sub> nanotube peeled off from the as-anodized sample, revealing a well-defined nanotubular structure. The spotless diffraction pattern in the inset confirms that the TaO<sub>x</sub> nanotubes are non-crystalline.

The previous study has reported that cell attachment, spreading, and cytoskeletal organization are significantly better on hydrophilic surfaces relative to hydrophobic surfaces [28]. Das et al. further indicated that a low contact angle implies high surface energy, which is also a crucial factor that contributes to better cell attachment [29]. It is thus essential to understand the influence of TaO<sub>x</sub> nanotube topography on the surface wettability. As shown in Fig. 4, all as-anodized TaO<sub>x</sub> nanotubes are highly hydrophilic since their contact angles are much smaller than 90°. Furthermore, their contact angles were found to monotonically decrease with decreasing nanotube diameter to 35 nm and then inversely increase as the diameter decreases to 20 nm. We also find that the TaO<sub>x</sub> nanotube samples show the similar trend when using either water or culture medium as testing liquids. We attempt to explain the observed wettability behavior based on Wenzel's law, which describes the small contact angle on hydrophilic materials [30]. In Wenzel's model, an increase of surface roughness in hydrophilic material will result in a smaller contact angle, and water will fill the grooves below the droplet. Here, we use the roughness factor, i.e., the physical surface area of nanotubes per unit of projected area, to evaluate the geometric roughness of TaO<sub>x</sub> nanotube samples [31]. As shown in Fig. 5, with

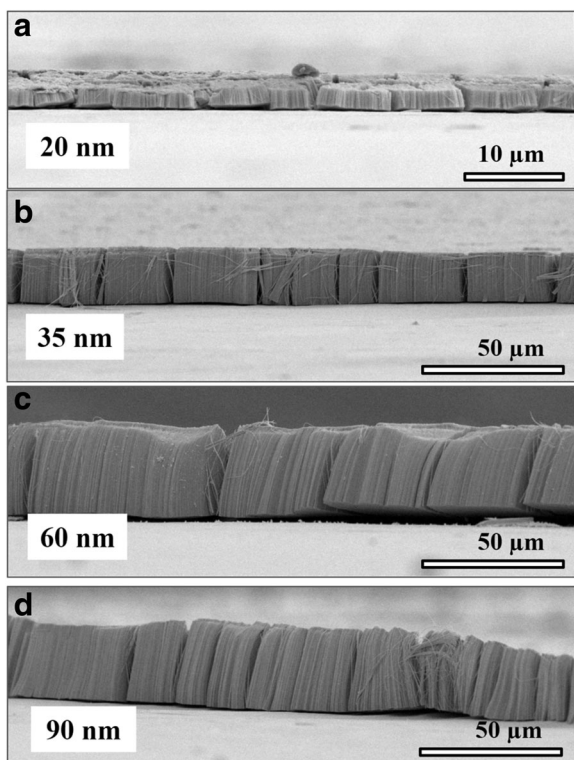


**Fig. 2** SEM images showing the cross-sections of TaO<sub>x</sub> nanotubes with diameters of **a** 20, **b** 35, **c** 65, and **d** 90 nm, respectively

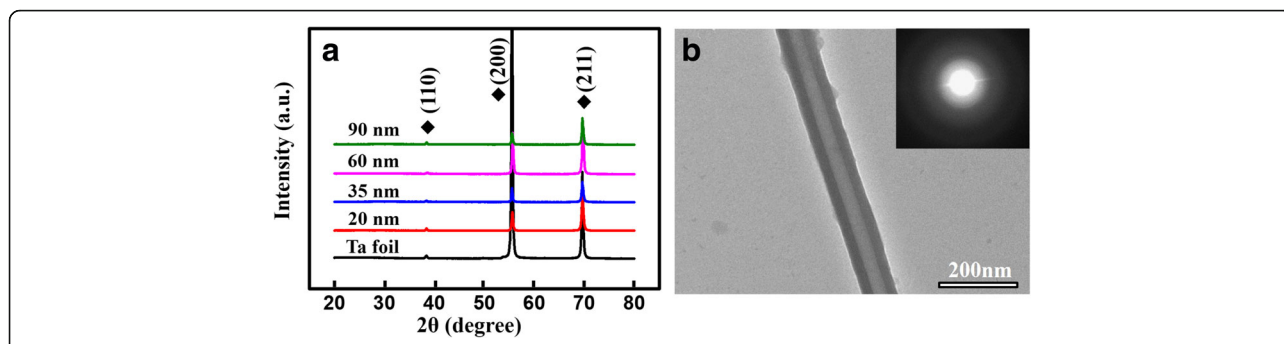


**Fig. 3** **a** XRD spectra of as-anodized TaO<sub>x</sub> nanotubes of different diameters and **b** TEM image taken from an as-anodized TaO<sub>x</sub> nanotube with the diameter of 90 nm. The inset also shows the corresponding diffraction pattern

inner diameter  $D$ , wall thickness  $W$ , and nanotube length  $L$ , the purely geometric roughness factor  $G$  can be calculated as  $[4\pi L\{D + W\}/\{\sqrt{3(D + 2W)^2}\}] + 1$ . This calculation assumes all surfaces of the nanotubes to be perfectly smooth. The calculated roughness factors for all nanotube samples are summarized in the table of Fig. 5. Except the 20-nm-diameter sample, the smaller diameter nanotubes have the larger geometric roughness and thus are thought to exhibit better hydrophilicity according to Wenzel’s model. This inference is consistent with our result that the contact angle decreases with decreasing nanotube diameter to 35 nm. It also well explains that the 20-nm-diameter nanotubes that exhibit relatively unclear nanotubular surface show smaller geometric roughness and poorer hydrophilicity than other ones.

The human fibroblast cell behavior in response to the flat Ta foil and TaO<sub>x</sub> nanotube arrays was further

studied. To evaluate the fibroblast cell attachment on the TaO<sub>x</sub> nanotubes, cytoskeleton actin was stained with rhodamine phalloidin to express red fluorescence and nuclei stained with DAPI to express blue fluorescence. The actin immunostaining shows distinguishable cell-material contact morphology for the flat Ta foil and TaO<sub>x</sub> nanotubes of different diameters (see Fig. 6). It is well known that cells have to adhere on material surface first and then spread for further cell division. Better cell adhesion can cause more activation of intracellular signaling cascades through integrin coupled to actin cytoskeleton [32–34]. FE-SEM was used for the detailed observation of cell adhesion (see Fig. 7). The fibroblasts on the 35-nm-diameter reveal excellent cell adhesion with an elongated flatten morphology. On the other hand, those fibroblasts on the Ta foil and 90-nm-diameter TaO<sub>x</sub> nanotubes show less attached cells and lack of cell spreading to some extent. The coverage area

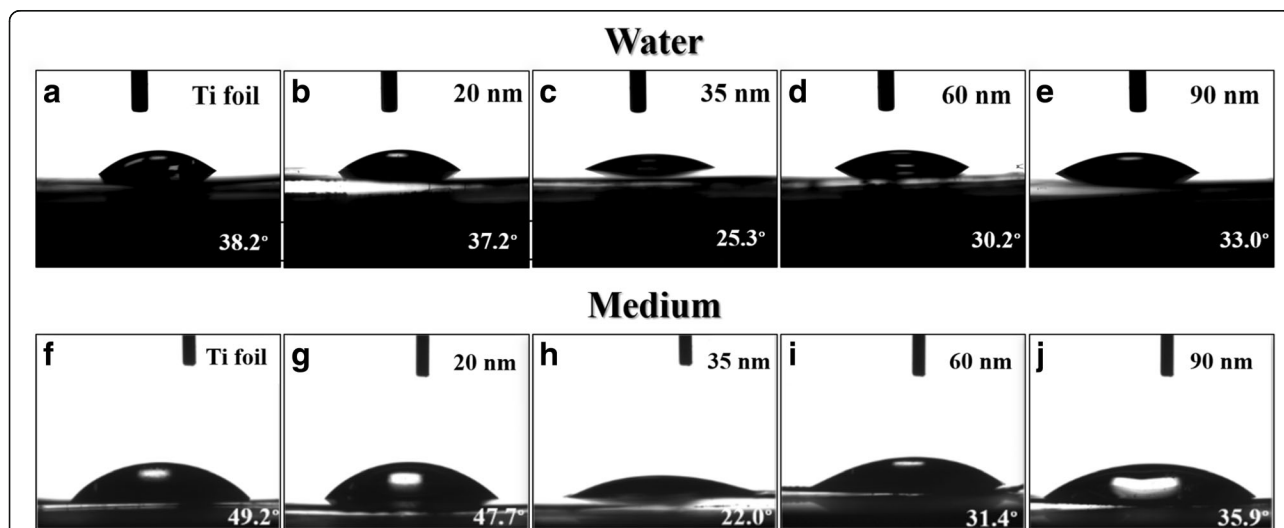
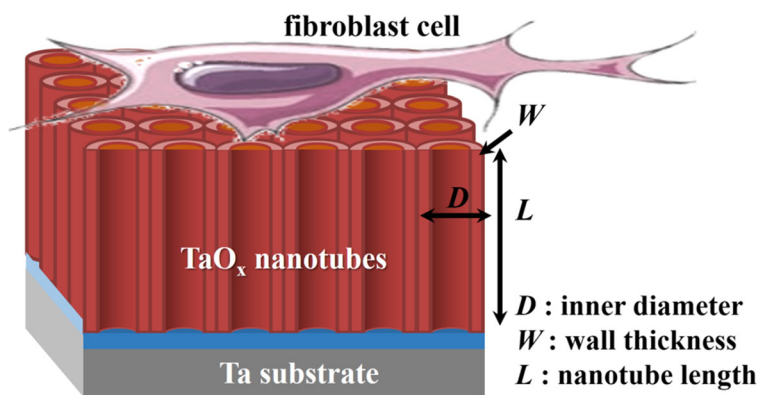


**Fig. 4** **a–j** Optical images showing water and culture medium droplets on the **a, f** Ta foil surface and self-organized TaO<sub>x</sub> nanotubes with diameters of **b, g** 20, **c, h** 35, **d, i** 65, and **e, j** 90 nm, respectively. Contact angles are denoted in the images



Nominal diameter (nm)	Inner diameter (nm)	Wall thickness (nm)	Nanotube length ( $\mu\text{m}$ )	Roughness factor (G)
90	88	42	18.4	590
60	61	39	30.3	1151
35	36	22	20.8	1399
20	21	15	2.1	209

**Fig. 5** Schematic diagram of an idealized nanotubular structure with inner diameter  $D$ , wall thickness  $W$ , and nanotube length  $L$ . The calculated roughness factors for all nanotube samples in this study are summarized in the table

of cells on the nanotubes was further estimated by using ImageJ software and noted in these SEM images. Similar to the trend of contact angles, the coverage area was found to monotonically decrease with decreasing nanotube diameter to 35 nm and then inversely increase as

the diameter decreases to 20 nm. The 35-nm-diameter  $\text{TaO}_x$  nanotube indeed shows the largest cell coverage area. It is known that cells recognize surface features when a suitable site for adhesion has been detected. It is supposed that cells can stable their contacts onto the

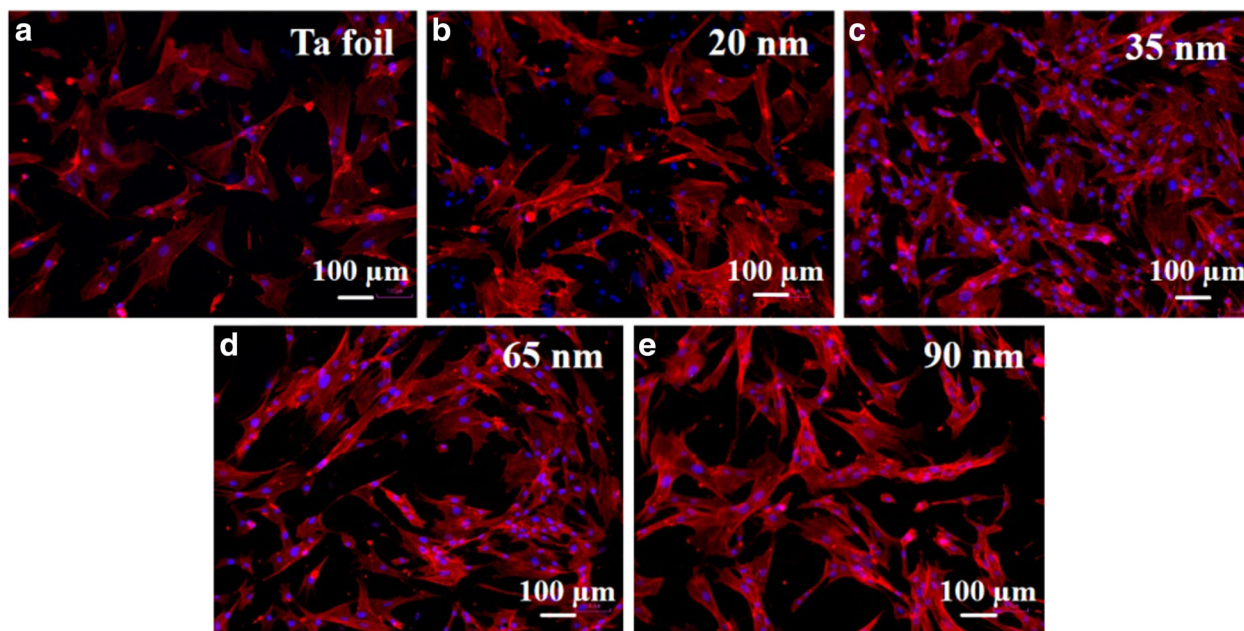
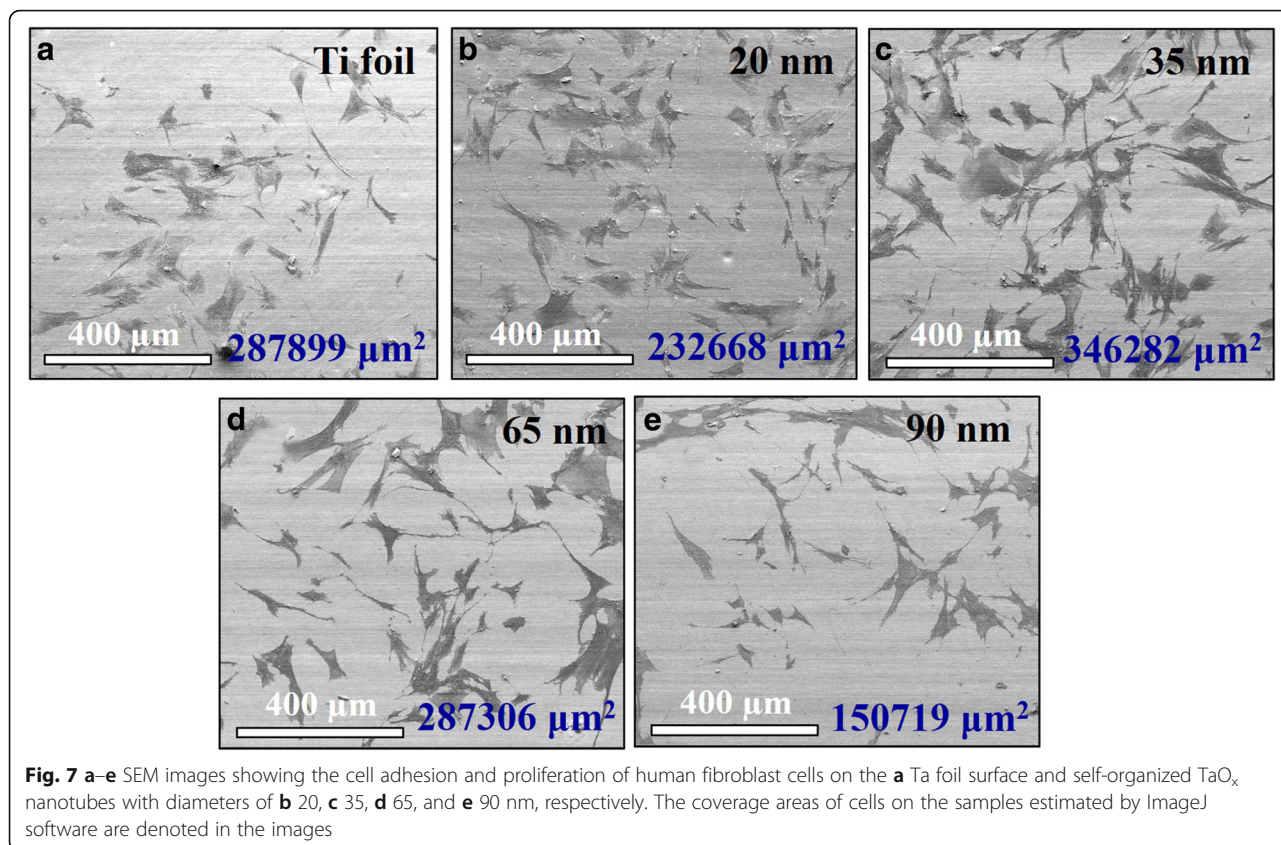


**Fig. 6** Fluorescence microscopy images of the fibroblast cell attachment on the **a** Ta foil and self-organized  $\text{TaO}_x$  nanotubes with diameters of **b** 20, **c** 35, **d** 65, and **e** 90 nm, respectively. The red fluorescence indicates cytoskeletal protein actin filament, and the blue fluorescence indicates nuclei

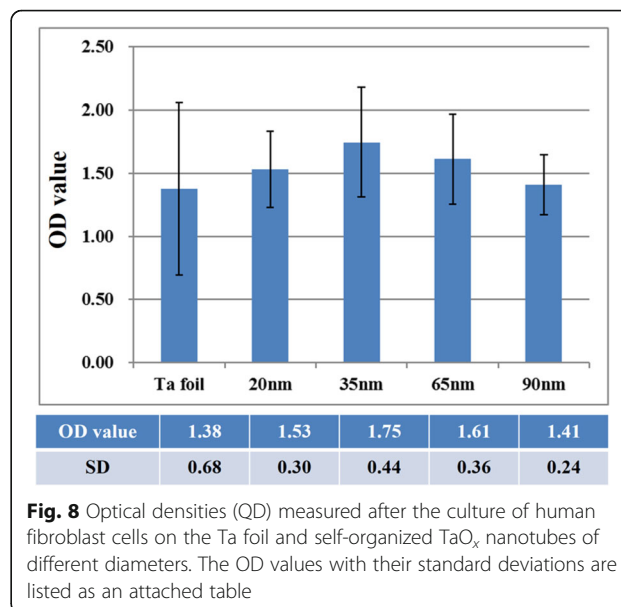


TaO<sub>x</sub> nanotubes by forming focal adhesions and mature actin fibers, followed by recruiting tubulin microtubules [35]. The actin cytoskeleton is linked to integrins which are located within the adhesions. Our findings suggest that the cytoskeleton on the 35-nm-diameter nanotubes could be formed better than those on the flat Ta foil or other TaO<sub>x</sub> nanotube arrays.

The WST-1 assay was employed to further evaluate the fibroblast cell proliferation on the TaO<sub>x</sub> nanotubes with different diameters. Figure 8 shows the comparison of optical densities measured from the WST-1 assay results. We find that cell proliferation is highest for the 35-nm-diameter TaO<sub>x</sub> nanotube sample. However, there is no significantly difference between Ta group and TaO<sub>x</sub> nanotube arrays. In addition, the cell proliferation and surface wettability exhibit a nearly similar trend with the TaO<sub>x</sub> nanotube diameters. This observation suggests that not only nanotube diameter but also surface wettability strongly influences the cell adhesion and the following spreading. In other words, compared to the 35-nm-diameter nanotubes, the 20-nm-diameter ones may give more focal points for fibroblast cells, but its poorer hydrophilicity eliminates some effective focal contacts and thus impedes the cell attachment. Eventually, the 35-nm-diameter TaO<sub>x</sub> nanotubes reveal the highest biocompatibility among all samples.

**Conclusions**

In conclusion, this work studies the biocompatibility of anodized TaO<sub>x</sub> nanotubes with different nanotube diameters. All anodized TaO<sub>x</sub> nanotubes were identified to be mainly amorphous phase. We discuss the transition in surface wettability with TaO<sub>x</sub> nanotube diameters based



on Wenzel's model. In vitro biocompatibility evaluation further indicates that fibroblast cells exhibit an obvious wettability-dependent behavior on the TaO<sub>x</sub> nanotube arrays. The 35-nm-diameter TaO<sub>x</sub> nanotube arrays reveal the best biocompatibility among all nanotube samples. This enhancement could be attributed to highly dense focal points provided by TaO<sub>x</sub> nanotubes due to higher surface hydrophilicity. This study demonstrates that the biocompatibility in Ta can be improved by forming TaO<sub>x</sub> nanotube arrays with appropriate nanotube diameter and geometric roughness.

#### Acknowledgements

The research was supported by the Ministry of Science and Technology of Taiwan under Contract No. 106-3113-E-008-003-CC2, 106-2314-B-075-035-MY3, and 106-2923-E-008-002-MY3, the Taipei Veterans General Hospital under Contract No. V106B-008, and National Central University under Contract No. NCU-LSH-106-B-. The authors also thank National Nano Device Laboratories for the facility support.

#### Authors' Contributions

YJZ, SCT, and KWW performed the preparation and material characterizations of all anodized TaO<sub>x</sub> nanotube samples. YJZ and SCT contributed equally to this work. HHH revised the manuscript. MYL, YBH, and CYW conducted the in vitro experiments and drafted the part of manuscript. SWL designed this study and wrote the manuscript. All authors read and approved the final manuscript.

#### Competing Interests

The authors declare that they have no competing interests.

#### Publisher's Note

Springer Nature remains neutral with regard to jurisdictional claims in published maps and institutional affiliations.

#### Author details

<sup>1</sup>Institute of Materials Science and Engineering, National Central University, Taoyuan 320, Taiwan, Republic of China. <sup>2</sup>Department of Dentistry, National Yang-Ming University, Taipei 11221, Taiwan, Republic of China. <sup>3</sup>Department of Otolaryngology Head and Neck Surgery, Taipei Veterans General Hospital, Taipei 112, Taiwan, Republic of China. <sup>4</sup>School of Medicine, National Yang-Ming University, Taipei 112, Taiwan, Republic of China. <sup>5</sup>Department of Emergency, Taipei Veterans General Hospital, Taipei 112, Taiwan, Republic of China.

Received: 18 June 2017 Accepted: 25 September 2017

Published online: 03 October 2017

#### References

- Sun YS, Chang JH, Huang HH (2013) Corrosion resistance and biocompatibility of titanium surface coated with amorphous tantalum pentoxide. *Thin Solid Film* 528:130–135
- MH O, Kim H, Park SP, Piao Y, Lee J, Jun SW, Moon WK, Choi SH, Hyeon T (2011) Large-scale synthesis of bioinert tantalum oxide nanoparticles for X-ray computed tomography imaging and bimodal image-guided sentinel lymph node mapping. *J Am Chem Soc* 133:5508–5515
- Matsuno H, Yokoyama A, Watari F, Uo M, Kawasaki T (2001) Biocompatibility and osteogenesis of refractory metal implants, titanium, hafnium, niobium, tantalum and rhenium. *Biomaterials* 22:1253–1262
- Schildhauer TA, Peter E, Köller M (2009) Activation of human leukocytes on tantalum trabecular metal in comparison to commonly used orthopedic metal implant materials. *J Biomed Mater Res* 88:332–341
- Tigani D, Sabbioni G, Raimondi A (2009) Early aseptic loosening of a porous tantalum knee prosthesis. *Musculoskelet Surg* 93:187–191
- Balla VK, Banerjee S, Bose S, Bandyopadhyay A (2010) Direct laser processing of a tantalum coating on titanium for bone replacement structures. *Acta Biomater* 6:2329–2334
- Balla VK, Banerjee S, Bose S, Bandyopadhyay A (2010) Porous tantalum structures for bone implants: fabrication, mechanical and in vitro biological properties. *Acta Biomater* 6:3349–3359
- Balla VK, Banerjee S, Bose S, Bandyopadhyay A (2010) Tantalum-A bioactive metal for implants. *J O M* 6:61–64
- Kim DG, Huja SS, Tee BC, Larsen PE, Kennedy KS, Chien HH, Lee JW, Wen HB (2013) Bone ingrowth and initial stability of titanium and porous tantalum. *Implant Dent* 4:399–405
- Maccaro G, Immetti PR, Muratori F, Raffaelli L, Manicone PF, Fabbrocoani C (2009) An overview about biomedical applications of micron and nano size tantalum. *Recent Pat Biotechnol* 3:157–165
- Stiehler M, Lind M, Mygind T, Bastrup A, Pirouz AD, Li H, Foss M, Besenancher F, Kassem M, Büniger C (2008) Morphology, proliferation, and osteogenic differentiation of mesenchymal stem cells cultured on titanium, tantalum, and chromium surfaces. *J Biomed Mater Res A* 86:448–458
- Hacking SA, Bobynd JD, Toh KK, Tanzer M, Krygier JJ (2000) Fibrous tissue ingrowth and attachment to porous tantalum. *J Biomed Mater Res* 52:631–638
- Ruckh T, Porter JR, Allam NK, Feng X, Girmes CA, Popatl KC (2009) Nanostructured tantalum as a template for enhanced osseointegration. *Nanotechnology* 20:045012–045018
- Tsao AK, Roberson JR, Christie MJ, Dore DD, Heck DA, Robertson DD, Poggie RA (2005) Biomechanical and clinical evaluations of a porous tantalum implant for the treatment of early-stage osteonecrosis. *J Bone Joint Surg Am* 87:22–27
- Levia BR, Sporera S, Poggie RA, Vallea CJD, Jacobsa JJ (2006) Experimental and clinical performance of porous tantalum in orthopedic surgery. *Biomaterials* 27:4671–4681
- Frigg A, Dougall H, Boyd S, Nigg B (2010) Can porous tantalum be used to achieve ankle and subtalar arthrodesis. *Clin Orthop Related Res* 468:209–216
- Cohen MM, Kazak M (2015) Tibiocalcaneal arthrodesis with a porous tantalum spacer and locked intramedullary nail for post-traumatic global avascular necrosis of the talus. *J Foot Ankle Surg* 54:1172–1177
- Sagomyants KB, Zargar MH, Jhaveri A, Aronow MS, Gronowicz G (2011) Porous tantalum stimulates the proliferation and osteogenesis of osteoblasts from elderly female patients. *J Orthop Res* 4:609–616
- Findlaya DM, Wellдона K, Atkina GJ, Howiea DW, Zannettinoc ACW, Bobybnb D (2004) The proliferation and phenotypic expression of human osteoblasts on tantalum metal. *Biomaterials* 25:2215–2227
- Yang H, Li J, Zhou Z, Ruan J (2013) Structural preparation and biocompatibility evaluation of highly porous tantalum scaffolds. *Mater Lett* 100:152–155
- Paganias CG, Tsakotos GA, Koutsostathis SD, Macheras GA (2014) The process of porous tantalum implants osseous integration a review. *Am J Med* 5:63–72
- Unger AS, Lewis RJ, Gruen T (2005) Evaluation of a porous tantalum uncemented acetabular cup in revision total hip arthroplasty. *J Arthroplast* 20:1002–1009
- Fairen MF, Murcia A, Blanco A, Meroño A, Ballester J (2010) Revision of failed total hip arthroplasty acetabular cups to porous tantalum components. *J Arthroplast* 25:865–872
- Meneghini RM, Ford KS, McCollough CH, Hanssen AD, Lewallen DG (2010) Bone remodeling around porous metal cementless acetabular components. *J Arthroplast* 25:741–744
- Macheras G, Kateros K, Kostakos A, Koutsostathis S, Danomaras D, Papagelopoulos PJ (2009) Eight- to ten-year clinical and radiographic outcome of a porous tantalum monoblock acetabular component. *J Arthroplast* 24:705–709
- Lin MY, Lee SL, Huang GG, Chen PF, Liu CP, Lee SW (2014) Diameter selective behavior of human nasal epithelial cell on Ag-coated TiO<sub>2</sub> nanotubes. *Ceram Int* 40:4745–4751
- Lan MY, Liu CP, Huang HH, Chang JK, Lee SW (2013) Diameter-sensitive biocompatibility of anodic TiO<sub>2</sub> nanotubes treated with supercritical CO<sub>2</sub> fluid. *Nanoscale Res Lett* 8:150–156
- Webb K, Hlady V, Tresos PA (1998) Relative importance of surface wettability and charged functional groups on NIH 3T3 fibroblast attachment, spreading, and cytoskeletal organization. *J Biomed Mater Res* 41:422–430
- Das K, Bose S, Bandyopadhyay A (2007) Surface modifications and cell-materials interactions with anodized Ti. *Acta Biomater* 3:573–585
- Wenzel RN (1936) Resistance of solid surfaces to wetting by water. *Ind Eng Chem Res* 28:988–994

31. Shankar K, Mor GK, Prakasam HE, Yoriya S, Paulose M, Varghese OK, Grimes CA (2007) Highly-ordered TiO<sub>2</sub> nanotube arrays up to 220 μm in length: use in water photoelectrolysis and dye-sensitized solar cells. *Nanotechnology* 18:065707
32. Dalby MJ, Childs S, Riehle MO, Johnstone HJH, Affrossman S, Curtis ASG (2003) Fibroblast reaction to island topography: changes in cytoskeleton and morphology with time. *Biomaterials* 24:927–935
33. Shekaran A, Garcia AJ (2011) Nanoscale engineering of extracellular matrix-mimetic bioadhesive surfaces and implants for tissue engineering. *Biochim Biophys Acta* 1810:350–360
34. Bjursten LM, Rasmusson L, Oh S, Smith GC, Brammer KS, Jin S (2010) Titanium dioxide nanotubes enhance bone bonding in vivo. *J Biomed Mater Res A* 92:1218–1224
35. Park J, Bauer S, von der Mark K, Schmuki P (2007) Nanosize and vitality: TiO<sub>2</sub> nanotube diameter directs cell fate. *Nano Lett* 7:1686–1691

**Submit your manuscript to a SpringerOpen<sup>®</sup> journal and benefit from:**

- ▶ Convenient online submission
- ▶ Rigorous peer review
- ▶ Open access: articles freely available online
- ▶ High visibility within the field
- ▶ Retaining the copyright to your article

---

Submit your next manuscript at ▶ [springeropen.com](http://springeropen.com)

---